JBC RESEARCH ARTICLE

Insulin-like growth factor binding protein-3 mediates hyperosmolar stress–induced mitophagy through the mechanistic target of rapamycin

Received for publication, September 3, 2022, and in revised form, July 29, 2023 Published, Papers in Press, September 9, 2023,
https://doi.org/10.1016/j.jbc.2023.105239

Whitney Stuard Sambhariya, Ian J. Trautmann, and Danielle M. Robertson*

From the Department of Ophthalmology, The University of Texas Southwestern Medical Center, Dallas, Texas, USA

Reviewed by members of the JBC Editorial Board. Edited by Alex Toker

Hyperosmolarity of the ocular surface triggers inflammation and pathological damage in dry eye disease (DED). In addition to a reduction in quality of life, DED causes vision loss and when severe, blindness. Mitochondrial dysfunction occurs as a consequence of hyperosmolar stress. We have previously reported on a role for the insulin-like growth factor binding protein-3 (IGFBP-3) in the regulation of mitochondrial ultrastructure and metabolism in mucosal surface epithelial cells; however, this appears to be context-specific. Due to the finding that IGFBP-3 expression is decreased in response to hyperosmolar stress *in vitro* and in an animal model of DED, we next sought to determine whether the hyperosmolar stress–mediated decrease in IGFBP-3 alters mitophagy, a key mitochondrial quality control mechanism. Here we show that hyperosmolar stress induces mitophagy through differential regulation of BNIP3L/NIX and PINK1-mediated pathways. In corneal epithelial cells, this was independent of p62. The addition of exogenous IGFBP-3 abrogated the increase in mitophagy. This occurred through regulation of mTOR, highlighting the existence of a new IGFBP-3–mTOR signaling pathway. Together, these findings support a novel role for IGFBP-3 in mediating mitochondrial quality control in DED and have broad implications for epithelial tissues subject to hyperosmolar stress and other mitochondrial diseases.

Dry eye disease (DED) is a chronic inflammatory disease of the ocular surface that, in severe forms, causes vision loss. DED has recently been defined in the dry eye workshop report as "a multifactorial disease of the ocular surface characterized by a loss of homeostasis of the tear film, and accompanied by ocular symptoms, in which tear film instability and hyperosmolarity, ocular surface inflammation and damage, and neurosensory abnormalities play etiological roles" (1). DED is broadly classified into two major subtypes: aqueous deficient and evaporative dry eye (1, 2). The former is due to a decrease in aqueous tear production by the lacrimal gland, while the latter results from a reduction in and/or abnormal lipid secretion by the meibomian glands. Regardless of the underlying etiology, both result in tear film instability and the induction of a hyperosmolar tear fluid. Hyperosmolarity in turn increases oxidative stress, inflammation, and apoptotic-mediated cell death. Mitochondrial dysfunction has also been implicated in the pathobiology of DED (3). We have previously reported that hyperosmolar stress promotes mitochondrial dysfunction in corneal and conjunctival epithelium, contiguous epithelia that together form the ocular surface. In addition to the eye, hyperosmolar stress has been linked to multiple disease pathologies, including asthma, inflammatory bowel disease, obesity, and hypernatremia (4–7).

The insulin-like growth factor binding protein-3 (IGFBP-3) is a pleiotropic protein with known roles in the inhibition of cell growth and survival (8). Indeed, during exponential growth, the addition of recombinant IGFBP-3 to proliferating corneal epithelial cells induces cell cycle arrest (9). In multiple epithelial cell types, however, we established a new role for IGFBP-3 in the modulation of mitochondrial structure and function in stressed cells (10). Importantly, we found that the loss of IGFBP-3 in corneal and conjunctival epithelial cells exposed to hyperosmolar stress was associated with a decrease in oxidative phosphorylation (11). Using a mouse model of aqueous-deficient DED, we similarly showed that IGFBP-3 expression was also decreased in the corneal epithelium (11, 12). The addition of exogenous IGFBP-3 blocked the hyperosmolar-mediated effects on mitochondrial function and dynamics, resulting in mitochondrial hyperfusion and an increase in oxidative phosphorylation *in vitro*. Exogenous IGFBP-3 also restored corneal epithelial cell health *in vivo* (12). Taken together, these data support a key role for IGFBP-3 as a stress response protein in the corneal and conjunctival epithelium. The mechanism by which IGFBP-3 mediates these mitochondrial effects is still unclear and may be significant for the development of novel therapies for certain mitochondrial diseases.

Autophagy is a well conserved mechanism that is essential to maintain homeostasis in cells exposed to an ever-fluctuating outside environment (13). Mitophagy, a form of selective autophagy, is the process in which the cell is able to eliminate damaged mitochondria (14). In order to undergo mitophagy, mitochondria first undergo fission to remove damaged regions. These mitochondrial fragments are then

* For correspondence: Danielle M. Robertson, Danielle.Robertson@UTSouthwestern.edu.

targeted for degradation in the lysosome through one of two principal pathways. The first is PINK1-PARKIN–mediated mitophagy, which is induced by mitochondrial depolarization and the subsequent accumulation of PINK1 in the outer mitochondrial membrane (15). The other is receptor-mediated mitophagy, whereby mitophagy receptors such as BNIP3, BNIP3L/NIX, AMBRA, and FUNDC1 are expressed on the outer mitochondrial membrane and directly recruit LC3 through their highly conserved LC3 interacting region motif (16). While early studies have implicated a potential role for autophagy in DED, the results to date are equivocal (17, 18). Not only is the role of autophagy in DED not well defined but the involvement of mitophagy in disease development and progression has not yet been explored.

The mechanistic target of rapamycin (mTOR) is a serine/threonine kinase that functions to regulate cellular metabolism, proliferation, protein translation, and autophagy. In prostate cancer, IGFBP-3 functions in a pro-apoptotic manner through the inhibition of the mTOR pathway (19). These findings conflict with our published data, as IGFBP-3 appears to be mitoprotective in cornea, conjunctival, and bronchial epithelial cells (10). Consistent with pleiotropic roles for IGFBP-3 in different cell types and settings, our unpublished data suggests that this mitoprotective effect may be context-specific. In the current study, we sought to determine the role if IGFBP-3 in the regulation of mitophagy during hyperosmolar stress. The potential ability of IGFBP-3 to mediate mitophagy would be consistent with the stark changes in mitochondrial phenotype. We now show that hyperosmolar stress increases mitophagy in corneal and conjunctival epithelial cells and that this occurs through the down-regulation of mTOR. We further demonstrate that the addition of exogenous IGFBP-3 can abrogate these mitochondrial effects through mTOR activation. This is associated with a robust enhancement in mitochondrial morphology and mitochondrial metabolism. Together, these findings indicate a new role for IGFBP-3 in the control of mitochondrial and metabolic homeostasis during hyperosmolar stress and demonstrate the existence of a new IGFBP-3–mTOR signaling pathway.

Results

Hyperosmolarity promotes autophagy in corneal and conjunctival epithelial cells

To determine the effect of hyperosmolarity on macroautophagy, corneal and conjunctival epithelial cells were treated with isotonic keratinocyte basal media (KBM) or KBM with increasing levels of osmolarity (450 mOsm or 500 mOsm) for 24 h. As a control, each condition was treated with or without bafilomycin-1 to block lysosomal fusion to the autophagosome. This results in the accumulation of autophagosomes. Immunoblotting for the microtubule-associated protein 1 A/1B-light chain (LC3) and the sequestosome 1 (P62/SQSTM1) in human corneal epithelial (hTCEpi) cells is shown in Figure 1*A*. There were no measurable changes in the expression of LC3-II or P62 in cells subjected to hyperosmolar stress (Fig. 1, *B* and *D*). In hTCEpi cells treated with bafilomycin, however, hyperosmolar stress led to an increase in LC3-II (Fig. 1*C*, $p < 0.05$ for 450 and 500 mOsm compared to isotonic KBM), indicating an increase in autophagy. Similarly, primary corneal epithelial cells also showed an increase in LC3-II during hyperosmolar culture after treatment with bafilomycin (Fig. 1, *E–G*, $p = 0.08$ and $p = 0.012$ for isotonic KBM compared to 450 and 500 mOsm, respectively). There were no measurable changes in P62 (Fig. 1*H*). The increase in autophagy in response to hyperosmolar stress was also seen in human conjunctival epithelial cells (HCjECs) treated with bafilomycin (Fig. 1, *I–L*). HCjECs showed a small reduction in LC3-II in cells cultured in hyperosmolar media (Fig. 1*J*, $p = 0.012$), whereas the addition of bafilomycin showed LC3 accumulation. While cells cultured in 450 mOsm showed a trend towards an increase in LC3-II, this effect was small and only significant at the higher test concentration (Fig. 1*K*, $p = 0.041$ in 500 mOsm). This suggests that the observed decrease in LC3-II found in cells without bafilomycin was due to an increase in autophagic flux. While P62 was unchanged by hyperosmolarity in HCjECs, it was increased in the presence of bafilomycin (Fig. 1*L*). This contrasts with our findings in both hTCEpi cells and human corneal epithelial cells (HCECs), suggesting that P62 is not a key autophagy adapter protein in corneal epithelial cells.

IGFBP-3 blocks autophagy in corneal and conjunctival epithelial cells subjected to hyperosmolar stress

Previous studies in our laboratory have demonstrated a role for IGFBP-3 in regulating macroautophagy and mitophagy in normal epithelial homeostasis (10). We next wanted to determine whether IGFBP-3 modulated autophagy in corneal and conjunctival epithelial cells exposed to hyperosmolar stress. To accomplish this, we quantified LC3-II expression levels in hTCEpi cells after 6 h of culture in 450 mOsm KBM. As reported above, in cells not treated with bafilomycin, there was no measurable change in LC3-II expression between isotonic KBM *versus* KBM supplemented to 450 mOsm (Figs. 2*A* and S1*A*). Cotreatment with recombinant human (rh) IGFBP-3, however, decreased expression of LC3-II ($p = 0.042$). In cells treated with bafilomycin, there was an increase in the accumulation of LC3-II in 450 mOsm media compared to isotonic KBM (Figs. 2*A* and S1*B*, $p = 0.005$). Again, cotreatment of these cells with rhIGFBP-3 attenuated LC3-II expression (Figs. 2*A* and S1*B*, $p = 0.019$). These data suggest that IGFBP-3 blocks autophagy in cells exposed to hyperosmolar stress. Similar findings were seen at the 24-h time point (Figs. 2*B* and S1, *D* and *E*). There were no significant changes in P62 expression between isotonic KBM and hyperosmolar-treated cells, with or without rhIGFBP-3 (Fig. S1, *C* and *F*). These changes were confirmed in HCjECs (Figs. 2*C* and S1, *G–I*) and in HCjECs (Figs. 2*D* and S1, *J–L*, $p < 0.05$).

To further interrogate changes in autophagic flux during hyperosmolar stress, we used an expression plasmid encoding GFP-mCherry-LC3. hTCEpi cells were transfected with the

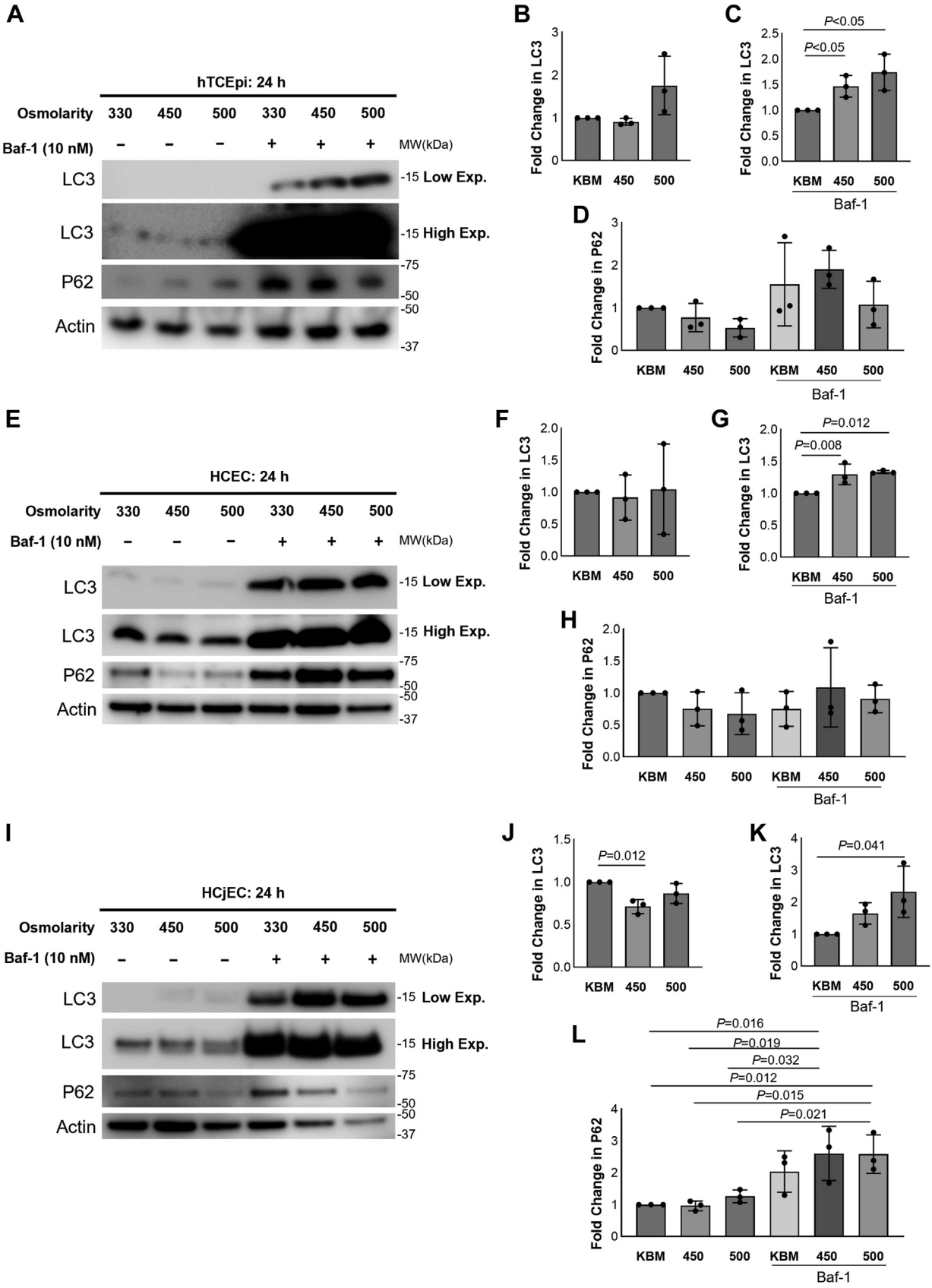

Figure 1. Hyperosmolarity promotes autophagy in corneal and conjunctival epithelial cells. *A–L*, cells were treated with isotonic KBM or KBM with an osmolarity of 450 mOsm or 500 mOsm for 24 h. Ten nanomolars of bafilomycin (Baf-1) was used to block lysosomal fusion in each condition. *A*, hTCEpi cell lysates were immunoblotted for P62 and LC3-II. Membranes were imaged using low (low exp) and high (high exp) exposure times to visualize the accumulation of LC3-II in cells treated with and without Baf-1, respectively. In the absence of Baf-1, no differences were observed in LC3-II. Hyperosmolar

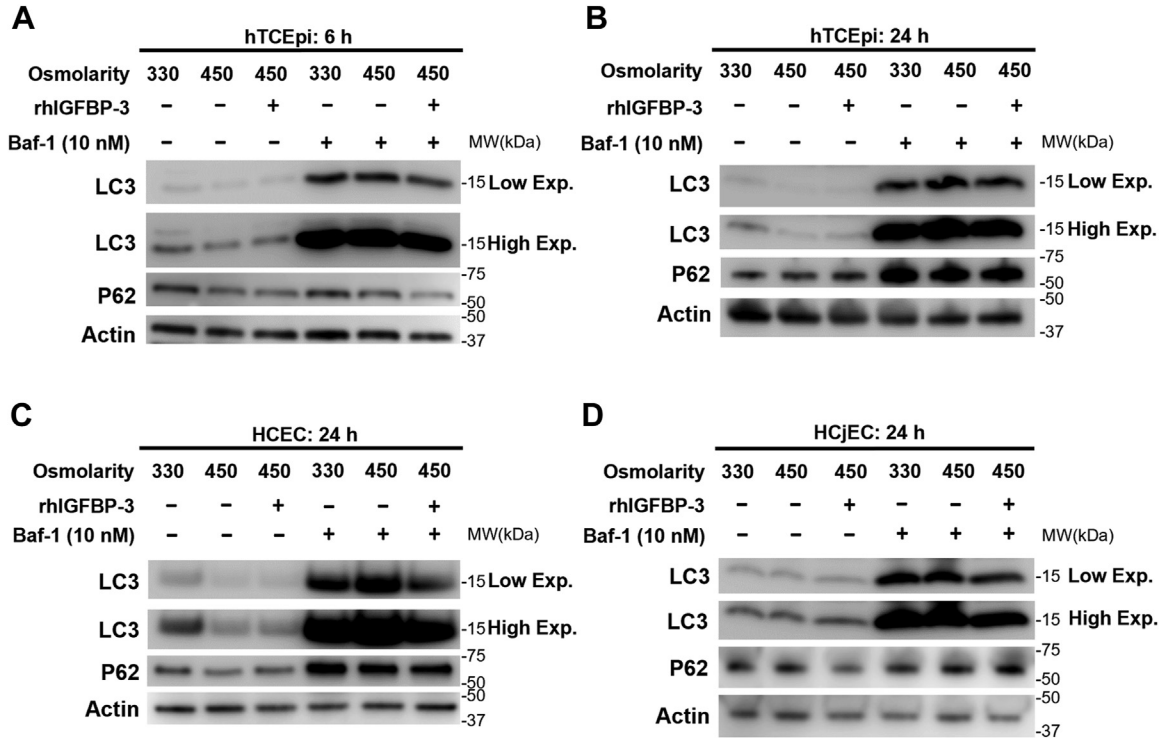

Figure 2. IGFBP-3 inhibits autophagy in ocular surface epithelial cells exposed to hyperosmolar stress. *A–D*, cells were treated with isotonic KBM or 450 mOsm KBM with or without 500 ng/ml rhIGFBP-3 for 6 or 24 h. Ten nanomolars of bafilomycin (Baf-1) was used to block lysosomal fusion. Cell lysates were blotted for P62 and LC3-II. *A*, after 6 h, cotreatment with rhIGFBP-3 decreased LC3-II levels in the absence of Baf-1. In the presence of Baf-1, hyperosmolar stress increased LC3-II levels; cotreatment with rhIGFBP-3 decreased LC3-II compared to 450 mOsm without rhIGFBP-3. *B*, after 24 h of culture, cells exposed to 450 mOsm showed an increase in LC3-II levels in Baf-1–treated cells; cotreatment with rhIGFBP-3 decreased LC3-II compared to 450 mOsm without rhIGFBP-3. *C*, in the presence of Baf-1, HCECs cotreated with rhIGFBP-3 had less LC3-II. *D*, HCjECs similarly showed no changes in LC3-II in the absence of Baf-1. Cells treated with Baf-1 had higher LC3-II expression in 450 mOsm KBM than isotonic KBM. Expression of LC3-II in HCjECs cotreated with rhIGFBP-3 was lower than KBM and 450 mOsm. β-actin was used as a loading control. low exp (low exposure); high exp (high exposure). Blots are representative of three repeated experiments. HCECs, human corneal epithelial cells; IGFBP-3, insulin-like growth factor binding protein-3; KBM, keratinocyte basal media; rh, recombinant human.

plasmid and then subsequently treated with isotonic KBM or 450 mOsm KBM with or without rhIGFBP-3 for 6 h. Consistent with our prior work using nonhyperosmolar stressed cells, there was an increase in the number of autophagosomes (yellow) and autophagolysosomes (red) in cells cultured in KBM compared to KGM at both 6 and 24 h (Fig. 3, *A–D*). Cells treated with 450 mOsm KBM showed an increase in autophagolysosomes (red) due to acidic degradation of GFP in the lysosome, demonstrating an increase in autophagic flux ($p < 0.05$). In cells cotreated with rhIGFBP-3, this increase in autophagolysosomes was not observed, consistent with a block in autophagy ($p < 0.05$).

IGFBP-3 mediates mitophagy through BNIP3L/NIX and PINK1 pathways

Due to the small changes in LC3, we hypothesized that these changes may be due to selective autophagy and not macroautophagy. To determine whether IGFBP-3 mediates mitophagy in corneal epithelial cells subjected to hyperosmolar stress, we first examined the BNIP3L/NIX and PINK1 pathways at 6 h by immunoblotting. As shown in Figure 4, *A* and *B*, there was an increase in BNIP3L/NIX expression in 450 mOsm KBM compared to isotonic KBM ($p = 0.04$). PINK1 also showed an increased trend in expression, suggesting potential stabilization of the protein at the outer mitochondrial membrane, although this increase was not significant (Fig. 4, *A* and *C*). Cotreatment with rhIGFBP-3 blocked the hyperosmolar-mediated increase in the expression of both BNIP3L/NIX and PINK1 in hTCEpi cells (Fig. 4*B*, $p = 0.008$ for BNIP3L/NIX; Fig. 4*C*, $p = 0.03$ for PINK1). Immunofluorescent staining for BNIP3L/NIX also showed an increase in fluorescence staining in cells under hyperosmolar stress (Figs. 4*D* and S4*A* $p < 0.05$). In agreement with the immunoblotting data, this increase was blocked by cotreatment with rhIGFBP-3. Immunofluorescent labeling for PINK1 in hTCEpi cells, while subtle, also showed an increase in cells exposed to hyperosmolar stress, which was similarly prevented by cotreatment with rhIGFBP-3 (Figs. 4*E* and S4*B* $p <$

stress increased expression of LC3-II in Baf-1–treated cells at both 450 and 500 mOsm ($p < 0.05$). *B–D*, quantification of immunoblots in (*A*). *E*, in HCECs, there was a similar increase in LC3-II in cells exposed to hyperosmolar stress in the presence of Baf-1 ($p = 0.008$ and $p = 0.012$ for 500 mOsm and 450 mOsm compared to isotonic KBM, respectively). *F–H*, quantification of immunoblots in (*E*). *I*, in HCjECs, LC3-II levels were increased in cells exposed to 500 mOsm when treated with Baf-1 ($p = 0.041$). *J–L*, quantification of immunoblots shown in (*I*). β-actin was used as a loading control. Data expressed as mean ± SD from three independent experiments. One-way ANOVA with Student-Newman-Keuls post hoc multiple comparison test. HCECs, human corneal epithelial cells; KBM, keratinocyte basal media.

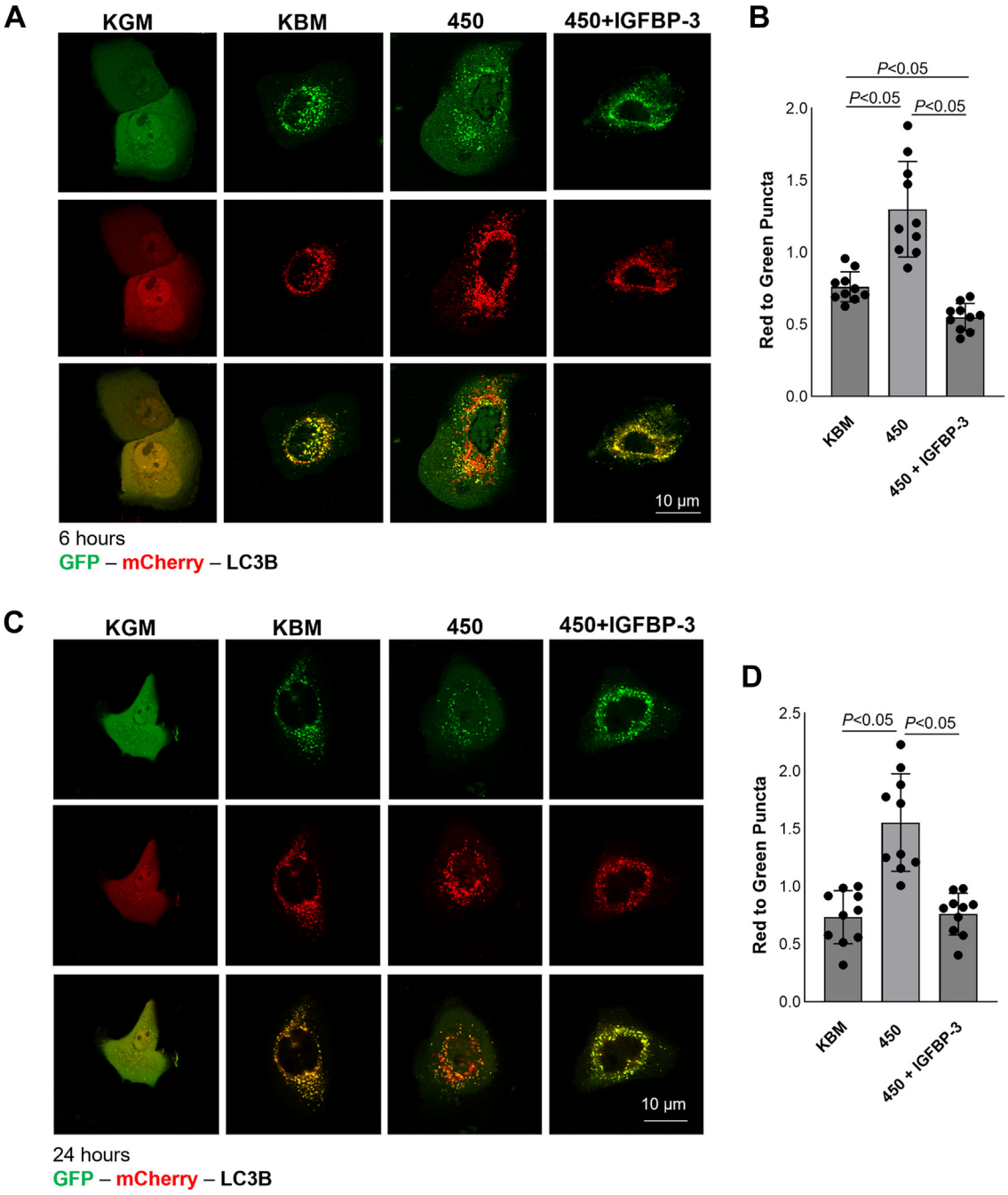

Figure 3. IGFBP-3 inhibits autophagic flux in corneal epithelial cells exposed to hyperosmolar stress. hTCEpi cells were transfected with a GFP-mCherry-LC3 expression plasmid. Cells were then cultured in either isotonic KBM or 450 mOsm KBM with or without 500 ng/ml rhIGFBP-3 for 6 or 24 h. *A*, at 6 h, there was an increase in the accumulation of autophagosomes (*yellow puncta*) and autophagolysosomes (*red puncta*) in KBM compared to the KGM control. Culture in 450 mOsm KBM increased the number of autophagolysosomes. Cells in 450 mOsm cotreated with rhIGFBP-3 had fewer autophagolysosomes than 450 mOsm without rhIGFBP-3. *B*, in 450 mOsm KBM, there was an increase in the ratio of red to green puncta compared to KBM ($p < 0.05$). In contrast, treatment with rhIGFBP-3 decreased the ratio of red to green puncta ($p < 0.05$). *C*, after 24 h in 450 mOsm KBM, there was a similar increase in autophagolysosomes. Again, cotreatment with rhIGFBP-3 led to an increase in autophagosomes, further suggesting a block in autophagic flux. *D*, similar to the 6 h time point, the ratio of red to green puncta was increased in cells cultured in 450 mOsm KBM at 24 h ($p < 0.05$). This was again decreased by treatment with rhIGFBP-3 ($p < 0.05$). Scale bar represents 10 μm. Images are representative of three repeated experiments. IGFBP-3, insulin-like growth factor binding protein-3; KBM, keratinocyte basal media; KGM, keratinocyte growth media; rh, recombinant human.

0.05). Since mitochondrial depolarization is required for PINK1 stabilization at the outer mitochondrial membrane, we next measured mitochondrial polarization in cells subjected to 6 h of hyperosmolar stress. We accomplished this using the J-aggregate–forming cationic dye (JC-1) (Figs. 4*F* and S4*C* (JC-1 monomer in green) and D (JC-1 aggregates in red), $p <$ 0.05) and colabeling mitochondria with MitoTracker Green (MTG) and tetramethylrhodamine ethyl ester (TMRE) (Figs. 4*G* and S4*E* (MTG) and F (TMRE) $p < 0.05$, respectively). Together, these data confirm that mitochondrial polarization was decreased in cells exposed to hyperosmolar stress, while cotreatment with rhIGFBP-3 maintained

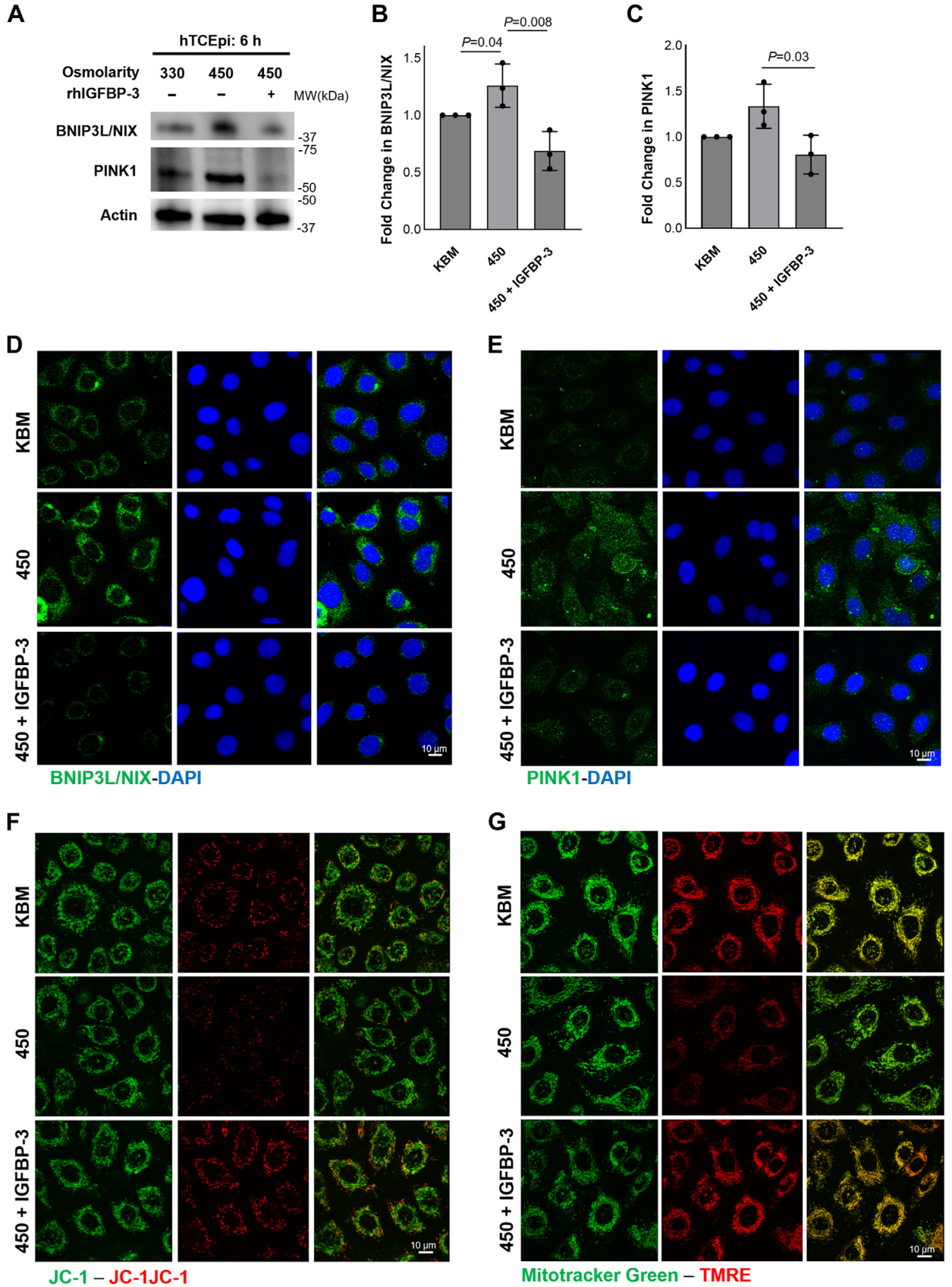

Figure 4. IGFBP-3 mediates mitophagy induced during acute hyperosmolar stress through BNIP3L/NIX and PINK1 pathways. Cells were cultured in isotonic KBM or 450 mOsm KBM with or without 500 ng/ml rhIGFBP-3 for 6 h. *A*, immunoblotting for mitochondrial proteins involved in mitophagy, BNIP3L/NIX and PINK1, in hTCEpi cells. ß-actin was used as a loading control. *B*, there was an increase in BNIP3L/NIX in 450 mOsm ($p = 0.04$), whereas cotreatment with rhIGFBP-3 decreased BNIP3L/NIX compared to 450 mOsm alone ($p = 0.008$). *C*, PINK1 was also decreased in rhIGFBP-3 cotreated cells ($p = 0.03$). *D* and

polarization near levels of isotonic KBM. These changes in polarization are consistent with the alterations in PINK1 expression. Thus, the increase in mitophagy during hyperosmolar stress is mediated through both PINK1 and BNIP3L/NIX pathways at this early time point.

To further investigate these mitophagy pathways, we next interrogated expression of BNIP3L/NIX and PINK1 after 24 h of hyperosmolar stress. In Figure 5*A*, hTCEpi cells were exposed to either isotonic KBM or 450 mOsm KBM with or without rhIGFBP-3. Similar to 6 h, BNIP3L/NIX expression was increased at 24 h in cells subjected to hyperosmolar stress compared to isotonic KBM (p = 0.021). This effect was again abrogated by cotreatment with rhIGFBP-3 (p = 0.032). In contrast, there was no change in PINK1 expression at 24 h of hyperosmolar stress. The changes in BNIP3L/NIX expression were confirmed in primary cultured HCECs (Fig. 5*B*). Immunofluorescent staining for BNIP3L/NIX paralleled the immunoblotting data, with an increase in fluorescence evident in the 24-h hyperosmolar stress group compared to isotonic KBM (Fig. 5, *C* and *E*, $p < 0.05$). This hyperosmolar stress-mediated increase in fluorescence was blocked by cotreatment with rhIGFBP-3 ($p < 0.05$). Finally, PINK1 immunofluorescent staining was largely unchanged at 24 h among the three groups (Fig. 5, *D* and *F*). Collectively, these data show that PINK-1–mediated mitophagy corresponds to early, acute changes in mitochondrial depolarization, whereas BNIP3L/NIX–mediated mitophagy is associated with the decrease in IGFBP-3 that is evident at both 6 and 24 h of hyperosmolar stress. Despite this difference in temporal activation, treatment with rhIGFBP-3 abrogated both mitophagy pathways.

IGFBP-3 mediates mitophagy through the mTOR pathway

To determine how treatment with rhIGFBP-3 blocks mitophagy, we examined levels of mTOR during hyperosmolar stress (Fig. 6, *A*–*C*). We found a sequential decrease in total mTOR expression that corresponded to increasing levels of osmolar stress (Fig. 6*B*, $p < 0.001$ for both 450 mOsm and 500 mOsm media compared to isotonic KBM). We further found a sequential decrease in mTOR phosphorylation at Ser(2448) (Fig. 6, *A* and *D*, p = 0.022 and p = 0.011 for 500 mOsm compared to 450 mOsm and isotonic KBM, respectively). This decrease in total mTOR expression was consistent with the increase in mitophagy seen with hyperosmolar stress (Fig. 1). As shown in Figure 6, *D*–*F*, when cells in 450 mOsm were cotreated with rhIGFBP-3, there was an increase in total mTOR compared to cells in 450 mOsm KBM (Fig. 6*E*, p = 0.049). There was no significant difference in the proportion of phosphorylated mTOR at Ser(2448) (Fig. 6*F*). Immunofluorescent staining corresponded to the immunoblotting data for total mTOR (Fig. 6, *G* and *I*, $p < 0.05$).

To further interrogate the relationship between IGFBP-3 and mTOR, we constitutively activated mTOR using siRNA to knockdown tuberous sclerosis complex 1 (TSC1). In parallel cultures, TSC1 knockdown cells and control cells were treated with either isotonic KBM, 450 mOsm KBM, or 450 mOsm KBM with rhIGFBP-3. Knockdown efficiency was measured by immunoblotting (Fig. 6*I*). A seahorse metabolic flux analysis was performed to measure the oxygen consumption rate (OCR). In cells treated with nontargeting oligonucleotides, there was a decrease in OCR in hTCEpi cells subjected to hyperosmolar stress (Fig. 6*J*, $p < 0.05$). This decrease was inhibited by treatment with rhIGFBP-3 (Fig. 6*J*, $p < 0.05$) (11). After siRNA knockdown of TSC1, OCR was unchanged during hyperosmolar stress. This indicates that the mTOR pathway modulates hyperosmolar changes in mitochondrial respiration in corneal epithelial cells. We next blocked mTOR activity using the mTOR pathway inhibitor, rapamycin. Once again, cells treated with vehicle controls in the absence of rapamycin showed the expected decrease in OCR during hyperosmolar stress (Fig. 6*K*, $p < 0.05$). Those treated with rapamycin, however, showed a sequential decrease in OCR in 450 mOsm KBM. This was further decreased in cells cotreated with rhIGFBP-3.

IGFBP-3 mediates mitochondrial morphology through the mTOR pathway

Using transmission electron microscopy, our lab previously showed that IGFBP-3 regulates mitochondrial ultrastructure and cristae maintenance, but the mechanism was undefined (10). As shown in Figure 7, cells cultured in KBM had sparse but morphologically intact mitochondria and cristae. During hyperosmolar stress, there was an increase in mitochondrial number, but mitochondria were small, suggestive of increased mitochondrial fission. Cristae in these mitochondria were wavy or missing (10). The presence of morphologically abnormal and missing cristae was consistent with the decrease in mitochondrial respiration found in cells exposed to hyperosmolar stress. As shown in Figure 7*B*, there was evidence of mitophagy in cells exposed to hyperosmolar stress, indicated by the presence of autophagosomes (white arrows) that contain or were forming around mitochondrial material. This supports the previously seen increase in autophagolysosomes using the GFP-mCherry-LC3B plasmid in Figure 3. Cotreatment with rhIGFBP-3, in contrast, showed elongated, hyperfused mitochondria with intact lamellar cristae. Cells treated with rapamycin, an mTORC1 inhibitor, also showed small mitochondria with abnormal cristae in 450 mOsm KBM; however, rapamycin blocked mitochondrial hyperfusion when cells were cotreated with rhIGFBP-3 (Fig. 7*A*). Using KU-0063794, an mTORC1 and 2 inhibitor, also blocked the effect of IGFBP-3

E, immunofluorescent labeling of hTCEpi cells for BNIP3L/NIX (*D*) and PINK1 (*E*). Nuclei were labeled with DAPI. Scale bar represents 10 μm. *F*, live-cell imaging using the mitochondrial polarization probe JC-1. JC-1 monomers (*green*) show mitochondria. Aggregates of JC-1 (*red*) represent areas of mitochondrial polarization. Scale bar represents 10 μm. *G*, live-cell imaging using the mitochondrial polarization probe TMRE and the mitochondrial probe MitoTracker Green. Scale bar represents 10 μm. Data presented as mean ± SD from three repeated experiments. One-way ANOVA with Student-Newman-Keuls post hoc multiple comparison test. IGFBP-3, insulin-like growth factor binding protein-3; KBM, keratinocyte basal media; rh, recombinant human; TMRE, tetramethylrhodamine ethyl ester.

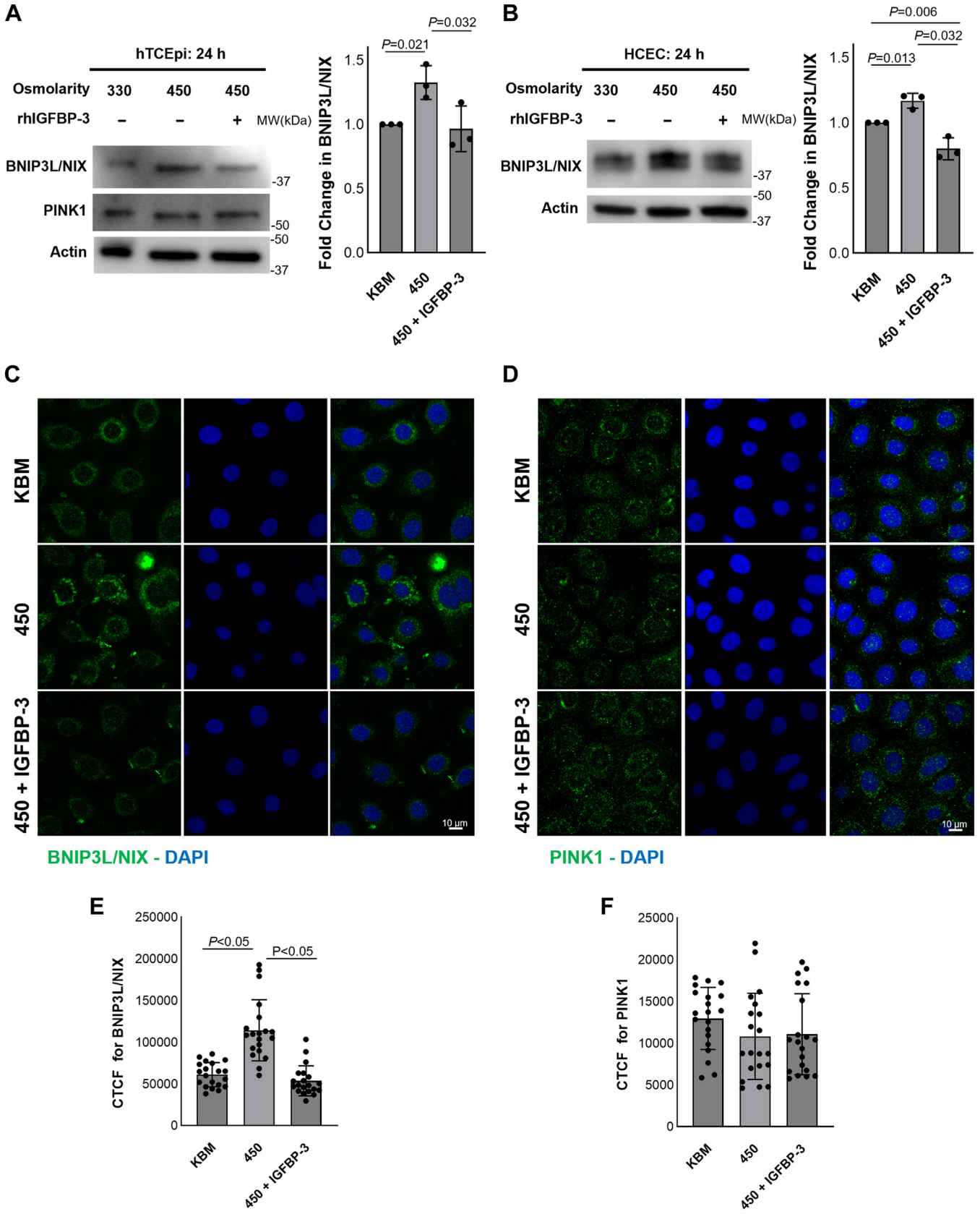

Figure 5. IGFBP-3 blocks mitophagy through BNIP3L/NIX at 24 h. Cells were cultured in isotonic KBM or 450 mOsm KBM with or without 500 ng/ml rhIGFBP-3 for 24 h. *A*, immunoblotting for BNIP3L/NIX and PINK1 in hTCEpi cells. There was an increase in BNIP3L/NIX in 450 mOsm (p = 0.021), whereas cotreatment with rhIGFBP-3 decreased BNIP3L/NIX compared to 450 mOsm (p = 0.032). PINK1 was unchanged. ß-actin was used as a loading control. *B*, immunoblotting of HCECs showed a similar pattern of expression for BNIP3L/NIX, with increased expression at 450 mOsm compared to the isotonic control (p = 0.013), which was then decreased by cotreatment with rhIGFBP-3 (p = 0.006 and p = 0.032; KBM and 450 mOsm compared to 450 with IGFBP-3,

on mitochondrial morphology (Fig. 7*C*). Taken together, these data indicate that a functional mTOR pathway is required for IGFBP-3 to promote mitochondrial hyperfusion and enhance lamellar cristae morphology.

Topical instillation of exogenous IGFBP-3 mediates mitophagy and mTOR in the mouse corneal epithelium during aqueous-deficient dry eye

To further investigate the effects of IGFBP-3 on mitophagy in the corneal epithelium, we used an aqueous-deficient dry eye mouse model (12). Phenol red thread testing was used to confirm a decrease in aqueous tear production and fluorescein staining of the corneal surface to quantify areas of epithelial damage (Fig. S2, *A*–*C*). Twenty-one days after the single dose botox injection, there was a significant decrease in tear production (p = 0.018, Fig. S2*A*). This corresponded to a significant increase in corneal staining (Fig. S2, *B* and *C*). We next examined expression levels of BNIP3L/NIX and PINK1 in the mouse corneal epithelium (Fig. 8). BNIP3L/NIX fluorescence was increased in mice with botox-induced DED and decreased after treatment with rhIGFBP-3 (Fig. 8*A*). The increase in BNIP3L/NIX was evident in the basal and suprabasal cell layers. We then analyzed PINK1 expression through immunostaining and found a similar increase in PINK1 in the superficial corneal epithelial cell layers in the botox-treated groups, with no effect on basal corneal epithelial cells. PINK1 expression across superficial epithelial cells was decreased in rhIGFBP-3–treated corneas (Fig. 8*B*). Finally, we examined the expression of mTOR and Ser(2448)-p-mTOR in the corneal epithelium of mice with and without botox (Figs. 8*C* and S3). Similar to our *in vitro* findings, botox-treated mice exhibited decreased fluorescence in total mTOR and Ser(2448)-p-mTOR that was restored by treatment with rhIGFBP-3.

Discussion

There are two key findings in this study. The first is that hyperosmolar stress induces both BNIP3L/NIX– and PINK1-mediated mitophagy. Using gain and loss of function assays *in vitro*, we have previously shown that IGFBP-3 mediates mitophagy in nonstressed corneal and conjunctival epithelial cells in cells subjected to growth factor withdrawal. Additional unpublished data in our laboratory, however, suggest that this effect is context-specific. Here, we used a hyperosmolar stress model and found an increase in autophagolysosomes by live-cell imaging and the subsequent accumulation of LC3-II on immunoblotting after treatment with bafilomycin. While these changes were small in magnitude, we did visualize an apparent increase in the number of small mitochondria visualized on electron microscopy, suggestive of mitochondrial fission. This led us to next examine two key mitophagy proteins, the mitophagy receptor BNIP3L/NIX and the mitochondrial Ser/Thr kinase PINK1, where we found an increase in the expression of both proteins in response to hyperosmolar stress *in vitro* and in our mouse aqueous-deficient dry eye model. These findings, coupled with the autophagic flux data, strongly supports the conclusion of an increase in mitophagy in response to hyperosmolar stress.

Importantly, there was a temporal difference in the expression of mitophagy proteins *in vitro*. Specifically, after 6 h (acute) of hyperosmolar stress, expression of both PINK1 and BNIP3L/NIX were increased. At the longer time point, however, the effect on PINK1 was lost. During normal homeostasis, PINK1 is transported to the inner mitochondrial membrane where it undergoes proteolytic cleavage and degradation. To maintain mitochondrial quality control, membrane depolarization triggers PINK1 accumulation on the outer mitochondrial membrane. PINK1 then recruits Parkin, an E3 ligase, to the mitochondria. Polyubiquitination follows, leading to LC3 recruitment and subsequent mitophagy to remove damaged regions of the mitochondria. The increase in PINK1 that was noted at the early time point is consistent with the change in mitochondrial polarization. As time progressed, the subsequent removal of damaged, depolarized mitochondria to regenerate the mitochondrial network would in turn promote the degradation of PINK1, reflected by the decrease in PINK1 expression. In contrast to this, BNIP3L/NIX expression remained high at the latter time point. This is likely due to the downregulation of IGFPB-3 that occurred early during hyperosmolar stress and was subsequently sustained throughout the duration of the stress. This is consistent with the finding that exogenous IGFBP-3 inhibited mitophagy in these cell types. Over time, this prolonged activation of BNIP3L/NIX-mediated mitophagy would trigger apoptotic cell death, a known consequence of hyperosmolar stress in the corneal epithelium (20, 21).

In vivo, we similarly found an increase in mitophagy in the corneal epithelium of mice with DED. Here, we found distinct spatial expression patterns for PINK1 and BNIP3L/NIX. BNIP3L/NIX was increased in the basal and suprabasal layers of the corneal epithelium, while PINK1 staining was increased in the apical layers. As the apical surface epithelial cells are subject to the highest level of hyperosmolar stress, the spatial restriction of PINK1-mediated mitophagy to the superficial corneal epithelial cell layers suggests that this is where the acute mitochondrial insult occurs. Indeed, PINK1 has been shown to play an important role in stress-mediated mitophagy, and a potential stress-sensing mechanism for PINK1-dependent mitophagy has been suggested (22). The increase in BNIP3L/NIX in the basal and immediately suprabasal layers of the corneal epithelium may reflect distinct physiological

respectively). *C* and *D*, immunofluorescent labeling of hTCEpi cells for (*C*) BNIP3L/NIX (*green*) was increased in cells treated with 450 mOsm compared to KBM ($p < 0.05$). This effect was blocked by cotreatment with rhIGFBP-3 ($p < 0.05$). *D*, there was no significant difference in PINK1 (*green*) expression at 24 h *E* and *F*, quantification of immunofluorescence in (*C*) and (*D*), respectively. Nuclei were labeled with DAPI. Scale bar represents 10 μm. Data presented as mean ± SD from three independent experiments. Images are representative of three repeated experiments. One-way ANOVA with Student-Newman-Keuls post hoc multiple comparison test. HCECs, human corneal epithelial cells; IGFBP-3, insulin-like growth factor binding protein-3; KBM, keratinocyte basal media; rh, recombinant human.

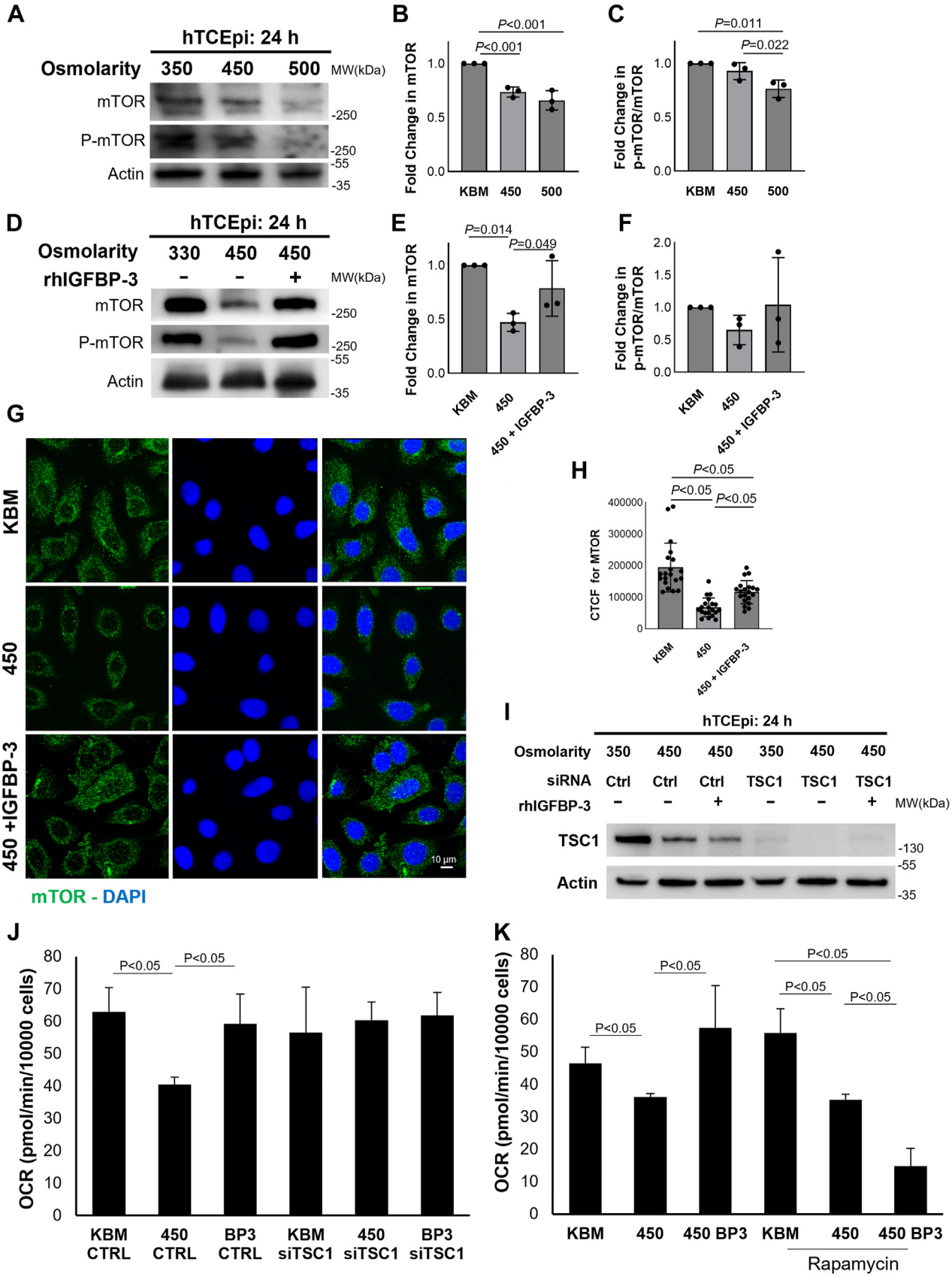

Figure 6. IGFBP-3 mediates the mTOR pathway to affect mitochondrial homeostasis. *A*, hTCEpi cells were cultured in KBM with increasing osmolarity (450 mOsm or 500 mOsm) for 24 h. Whole cell lysates were immunoblotted for mTOR and Ser(2448)-p-mTOR. As osmolarity increased, both mTOR ($p <$ 0.001) and p-mTOR ($p = 0.011$ and $p = 0.022$) were sequentially decreased. *B* and *C*, quantification of immunoblots in (*A*). *D*, cells were cultured in isotonic KBM or 450 mOsm KBM with or without 500 ng/ml rhIGFBP-3 for 24 h. Cell lysates were again immunoblotted for mTOR and Ser(2448)-p-mTOR. In 450

differences between cells in these layers and not direct hyperosmolar stress–induced damage (23). Instead, we propose that BNIP3L/NIX mediates preprogrammed mitophagy that occurs as a consequence of differentiation in corneal epithelial cells. This is consistent with prior work describing a role for BNIP3L/NIX mitophagy during cellular differentiation and maturation (24). Moreover, in a mouse model of desiccating stress, it has previously been shown that damage or desquamation of the surface epithelium is associated with an increase in proliferation of basal epithelial cells that are needed to replenish the full thickness epithelium (25). Our own unpublished data confirms an increase in basal cell proliferation in the botox-DED model used in this study. Thus, BNIP3L/NIX mitophagy may be an important component in mediating proliferation and vertical differentiation of these cells. Further work is needed to investigate these different signaling pathways.

The second key finding in this study is the regulation of mTOR by exogenously applied IGFBP-3. In our prior work, we found that treatment of epithelial cells with IGFBP-3 during hyperosmolar stress was sufficient to restore metabolic activity and promote mitochondrial hyperfusion (11, 12). This was associated with an increase in the mitochondrial fusion protein, MFN2 (22). The mechanism by which IGFBP-3 exerted these effects was unknown. We now show that IGFBP-3 blocks mitophagy mediated by both PINK1 and BNIP3L/NIX. We further show, for the first time, that IGFBP-3 negatively regulates mTOR in our cell culture model and in our mouse DED model. The ability of mTOR to regulate macro and selective autophagy is well established (26, 27). What is of greater interest, however, is the ability of mTOR inhibitors to blunt the effects of IGFPB-3 on mitochondrial respiration. Not only was respiration unaffected but the inhibition of mTOR blocked IGFBP-3–induced mitochondrial hyperfusion and the enhancement in lamellar cristae architecture. Since the electron transport chain is localized within the cristae, the loss of lamellar cristae may explain the reduction in respiration. In contrast to this, constitutive activation of mTOR by knockdown of TSC1 overrode the hyperosmolar decrease in respiration. In this latter case, IGFBP-3 was unable to further activate mTOR. Together, these data demonstrate that a functional mTOR signaling pathway is required for the mitoprotective effects of IGFBP-3.

In summary, these findings indicate that PINK1 and BNIP3L/NIX mitophagy pathways differentially regulate the cellular response to hyperosmolar stress. PINK1 functions to mediate acute hyperosmolar stress in differentiated epithelial cells at the ocular surface, whereas BNIP3L/NIX plays a key role in basal mitophagy in mitotic and early postmitotic cells. These data support the need for future work to determine whether BNIP3L/NIX is indeed involved in the programmed removal of mitochondria during epithelial differentiation and the role of dysregulation of this pathway in the pathophysiology of disease. Importantly, these data also show that both mitophagy pathways are negatively regulated by IGFBP-3 through modulation of mTOR, which in turn results in diverse mitochondrial phenotypes that correspond to energy production. Given the broad implications for epithelial surfaces exposed to hyperosmolar stress, the determination of how IGFBP-3 regulates mTOR to drive mitochondrial ultrastructure is a crucial topic that warrants further investigation.

Experimental procedures

Cell lines and culture

Two human telomerase-immortalized epithelial cell lines were used for these experiments. The hTCEpi cell line immortalized with hTERT was established and characterized by our laboratory (28). The HCjEC cell line, immortalized with hTERT, mutant Cdk4, and dominant-negative p53, was provided by Drs Pablo Argüeso (Schepens Eye Research Institute, Harvard Medical School) and Ajay Sharma (School of Pharmacy, Chapman University) (29–32). All cells were maintained at 37 °C with 5% CO_2 in serum-free KBM with growth factor supplements (KGM, Keratinocyte Growth Medium 2, PromoCell, VWR). Calcium was maintained at 0.15 mM using the manufacturer-recommended calcium chloride solution (PromoCell, VWR). Primary cultures were established from donor corneas provided by Tissue Transplant Services at UT Southwestern Medical Center. All primary corneal epithelial cells (HCECs) were harvested and cultured as previously described (33). Briefly, HCECs were initially cultured on Type IV collagen–coated plates (Corning) in CnT20 cell culture media enriched for progenitor cell culture (Zen Bio, Research Triangle Park). After the first passage, HCECs were transitioned to serum-free KGM media in tissue culture–treated T75 flasks. Osmolarity of the media, as provided by the manufacturer, is approximately 330 mOsm. For hyperosmolar cultures, media was supplemented with NaCl (Thermo Fisher Scientific).

Reagents

rhIGFBP-3 was acquired through Sino Biological and used at a concentration of 500 ng/ml. The lyophilized protein was

mOsm KBM, mTOR was decreased ($p = 0.014$). This decrease was blocked by cotreatment with rhIGFBP-3 ($p = 0.049$). Despite a similar trend, changes in p-mTOR were not significant. Total mTOR was used as a loading control for Ser(2448)-p-mTOR. ß-actin was used as a loading control for mTOR. *E* and *F*, quantification of immunoblots in (*B*). *G*, immunofluorescent labeling of hTCEpi cells for mTOR (*green*) at 24 h. Nuclei were labeled with DAPI. Scale bar represents 10 μm. *H*, quantification of immunofluorescence in (G). *I* and *J*, hTCEpi cells were transfected with siRNA oligonucleotides targeting TSC1 or a nontargeting control. Cells were treated with isotonic KBM, 450 mOsm KBM, or 450 mOsm KBM with 500 ng/ml rhIGFBP-3. *I*, knockdown efficiency was confirmed using immunoblotting for TSC1. ß-actin was used as a loading control. *J*, mitochondrial oxygen consumption was significantly decreased in cells treated with 450 mOsm ($p < 0.05$) and restored to basal levels upon cotreatment with rhIGFBP-3 ($p < 0.05$). TSC1 knockdown cells showed no differences in OCR. *K*, cells were cultured in 450 mOsm KBM with or without rhIGFBP-3. Cells treated with rapamycin, an mTOR inhibitor, were cultured in parallel. Treatment with rapamycin showed significant decreases in OCR compared to nonrapamycin-treated cells ($p < 0.05$). Data expressed as mean ± SD from one representative experiment, n = 3. One-way ANOVA with Student-Newman-Keuls post hoc multiple comparison test. IGFBP-3, insulin-like growth factor binding protein-3; KBM, keratinocyte basal media; mTOR, mechanistic target of rapamycin; OCR, oxygen consumption rate; rh, recombinant human; TSC1, tuberous sclerosis complex 1.

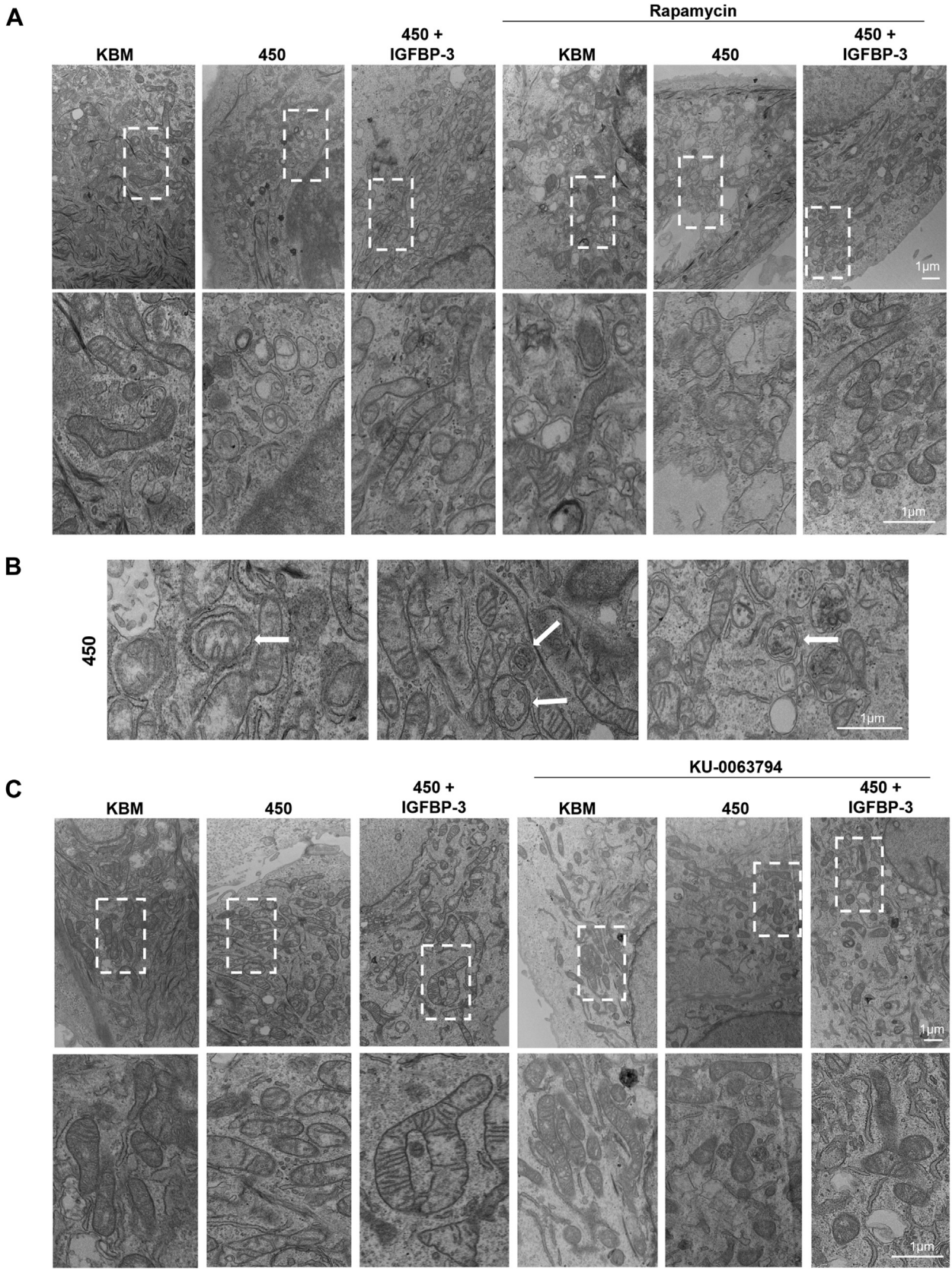

Figure 7. Inhibition of mTOR blocks IGFBP-3–mediated mitochondrial hyperfusion. hTCEpi cells were cultured in isotonic KBM or 450 mOsm KBM with or without 500 ng/ml rhIGFBP-3 for 24 h. TEM shows distinct changes in mitochondrial morphology and lamellar structure across treatment groups. *A*, treatment with rapamycin blocked IGFBP-3–mediated hyperfusion. *B*, TEM demonstrating mitophagy in hTCEpi cells subject to hyperosmolar stress. *C*, similar to rapamycin, treatment with KU-0063794 blocked IGFBP-3–mediated hyperfusion. Scale bar represents 1 μm. IGFBP-3, insulin-like growth factor binding protein-3; KBM, keratinocyte basal media; mTOR, mechanistic target of rapamycin; rh, recombinant human.

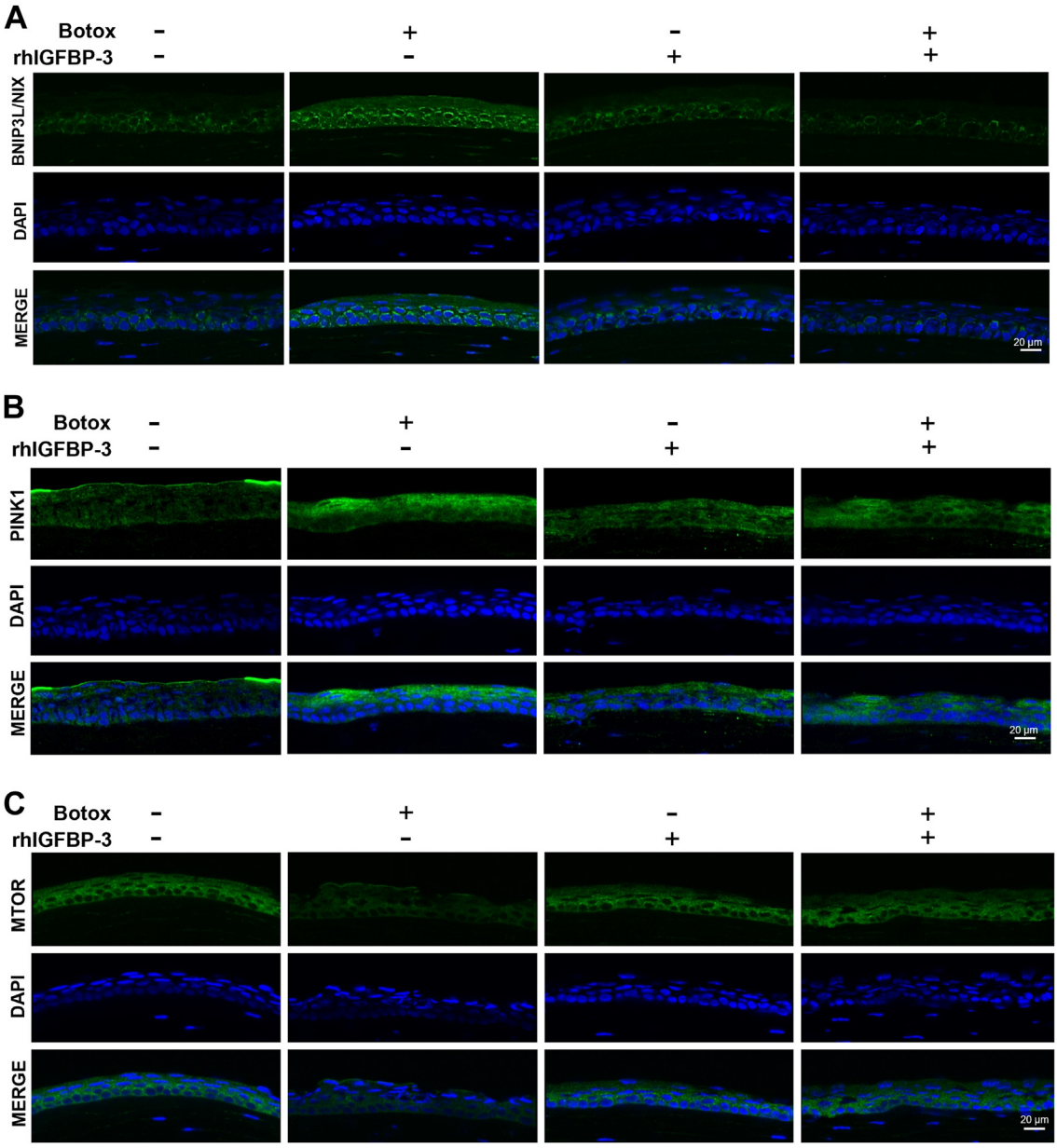

Figure 8. IGFBP-3 regulates mitophagy and mTOR in the corneal epithelium in dry eye disease. The mouse lacrimal gland was injected with botulinum toxin or a vehicle control. Twenty-one days postinjection, mice were treated topically twice a day every other day for 7 days with 10 μl of sterile saline with or without 500 ng/ml rhIGFBP-3. Immunostaining of cryo-sectioned corneas for (*A*) BNIP3L/NIX (*green*), (*B*) PINK1 (*green*), and (*C*) mTOR (*green*). Nuclei were counterstained with DAPI (*blue*). Scale bar represents 20 μm. Images are representative of three or more mice per group. IGFBP-3, insulin-like growth factor binding protein-3; mTOR, mechanistic target of rapamycin; rh, recombinant human.

resuspended using ultrapure water according to manufacturer instructions. Two mTOR inhibitors were used, rapamycin (Thermo Fisher Scientific) and KU-0063794 (Sigma). Antibodies used for immunoblotting and immunofluorescence included the following: a rabbit monoclonal anti-mTOR #2983, a rabbit polyclonal anti-phospho-mTOR (Ser2448) #2971, a rabbit monoclonal anti-BNIP3L/NIX #12396, a mouse polyclonal anti-β-actin #sc-47778, a rabbit monoclonal antibody anti-Hamartin/TSC1 #6935 (Cell Signaling Technology); a rabbit polyclonal anti-LC3B #L7543 (Sigma); a mouse monoclonal anti-p62/SQSTM1 #H00008878 (Novus Biologicals); a rabbit polyclonal anti-PINK-1 #AB23707 (Abcam), and a mouse monoclonal anti-LC3B #M152-3 (MLB). Secondary antibodies for immunoblotting included a goat anti-rabbit IgG conjugated to horseradish peroxidase #170-6515 and goat anti-mouse conjugated to horseradish peroxidase #170-6516 (Bio-rad). Secondary antibodies for immunofluorescence included an anti-rabbit IgG conjugated to Alexa Fluor 488 and anti-mouse IgG conjugated to Alexa Fluor 555 (Cell Signaling Technology).

Real-time metabolic studies

A Seahorse Metabolic Flux Analyzer (Agilent Technologies) was used to measure cellular OCR and intracellular acidification rate simultaneously under various conditions. hTCEpi cells were seeded onto Seahorse XFp miniplates and allowed to

adhere overnight at 37 °C, 5% CO_2 for 24 h. The media was then removed and the Seahorse miniplates were treated with isotonic KBM or KBM supplemented to 450 mOsm with or without rhIGFBP-3. For mTOR studies, each of these conditions were treated with or without an mTOR inhibitor, KU-0063794 or rapamycin, for an additional 24 h at 37 °C, 5% CO_2. Following that incubation, all media was removed and replaced with Seahorse XF base medium containing 1 mM pyruvate, 2 mM glutamine, and 10 mM glucose (pH 7.4). Cells were incubated for 1 h at 37 °C in a non-CO_2 incubator. A Cell Mito Stress Test Kit (Agilent Technologies) was used to analyze mitochondrial metabolism. The run time was 94 min with measurements taken at 6-min intervals. At 20 min, 10 μM oligomycin was injected to inhibit ATP synthase. Next, at 50 min, 10 μM carbonyl cyanide 4-(trifluoromethoxy) phenylhydrazone was injected to uncouple the electron transport chain proton gradient allowing for maximal respiration due to unimpeded electron flow. Finally, at 80 min, rotenone and antimycin A were injected to block complexes 1 and 3 of the electron transport chain, respectively. This inhibited mitochondrial respiration and allowed for the analysis of non-mitochondrial respiration. The results were analyzed using the manufacturer's provided Wave software (https://www.agilent.com/en/product/cell-analysis/real-time-cell-metabolic-analysis/xf-software/seahorse-wave-desktop-software-740897), version 2.3.0. All wells were normalized by cell number obtained by direct count using a Celigo Imaging Cytometer (Nexcelom Bioscience). All experiments were repeated a minimum of two additional times. Of note, the following parameters were calculated as described: spare respiratory capacity = (maximal respiration)/(basal respiration) ×100 and coupling efficiency = (ATP-linked respiration rate)/(basal respiration rate) ×100.

Transmission electron microscopy

For these experiments, hTCEpi cells were seeded at 70% confluence onto 35 mm glass-bottom dishes (MatTek Corporation) and allowed to adhere overnight. Cells were treated with KBM, KBM at 450 mOsm, or KBM at 450 mOsm with rhIGFBP-3. For mTOR studies, each of these conditions were then treated with or without an mTOR inhibitor, either KU-0063794 or rapamycin, for 24 h at 37 °C, 5% CO_2. After this treatment, cells were fixed at room temperature for 15 min with a solution of 2.5% glutaraldehyde/0.1 M cacodylate buffer pH 7.4. Cells were washed three times for 5 min with a solution of 0.1 M sodium cacodylate buffer. They were then postfixed with 1% osmium tetroxide and 0.8 % $K_3[Fe(CN_6)]$ in 0.1 M sodium cacodylate buffer for 1 h at room temperature and rinsed with water. Cells were stained overnight *en bloc* with 2% aqueous uranyl acetate. The next day, cells were rinsed with water and then dehydrated by adding increasing concentrations of ethanol. Cells were infiltrated by embed-812 resin and allowed to polymerize overnight at 60 °C. Cell blocks were sectioned using a diamond knife (Diatome Knives) on a Leica Ultracut UCT (7) ultramicrotome (Leica Microsystems). Sections were dispersed onto copper grids, which were post-stained with 2% uranyl acetate in water and lead citrate. A JEOL 1400 Plus (JEOL) equipped with a LaB_6 source using a voltage of 120 kV was used to acquire images from the sections.

SDS-PAGE and immunoblotting

A lysate buffer with a phosphatase protease inhibitor cocktail (Thermo Fisher Scientific) was used to directly lyse epithelial cells for immunoblotting. The lysis buffer was made of 50 mM Tris–HCl pH 7.5, 150 mM NaCl, 1% Triton X-100, and 1 mM EDTA. Whole cell lysates were placed on ice for 10 min and then centrifuged at 12,000 rpm for 5 min at 4 °C after which the supernatants were removed. The protein concentration of each supernatant was measured using a Qubit 3.0 Fluorometer (Thermo Fisher Scientific). 2 ×sample buffer pH 6.8 containing 65.8 mM Tris–HCl, 26.3% (w/v) glycerol, 2.1% SDS, 5.0% β-mercaptoethanol, and 0.01% bromophenol blue (Bio-rad) was added to each sample and immediately boiled for 5 min. Samples were then loaded and electrophoresed through a 4 to 15% precast linear gradient polyacrylamide gel (Bio-rad). Gels were transferred to a polyvinyl difluoride membrane which was equilibrated using methanol (Millipore). After transfer, the membrane was placed in 5% nonfat milk (Bio-rad) for 1 h at room temperature. After 1 h, membranes were washed three times for 5 min with PBS. Membranes were incubated at 4 °C overnight in primary antibodies followed by washing in PBS. Finally, membranes were incubated with anti-mouse or anti-rabbit secondary antibodies and washed prior to imaging (Santa Cruz). ECL Prime Detection Reagent (Amersham Biosciences) was used to visualize protein using an Amersham Imager 600 (Amersham Biosciences). β-actin or GAPDH were used as loading controls for immunoblotting. ImageQuant TL Toolbox v8.1 software (Amersham Bioscience) was used to quantify protein bands. Phosphorylated proteins were normalized to the respective total protein. To allow for statistical analysis, all experiments were repeated a minimum of two independent times.

Immunofluorescence

For *in vitro* studies, hTCEpi cells were seeded at 70% confluence onto 35 mm glass-bottom dishes (MatTek Corporation) and allowed to adhere overnight in KGM. The media was then removed and replaced with isotonic KBM (basal) or 450 mOsm KBM with or without rhIGFBP-3. Cells were cultured for 6 or 24 h. After treatment, cells were washed with cold PBS twice and fixed using 1% paraformaldehyde in PBS (Electron Microscopy Sciences) for 10 min. Cells were again washed with PBS and permeabilized with 0.1% Triton X-100 in PBS for another 10 min. Cells were then washed in PBS three additional times and blocked using 0.5% bovine serum albumin in PBS (Sigma) for 30 min at room temperature. Cells were incubated in primary antibody diluted in 0.1% bovine serum albumin (Sigma) and placed in 4 °C overnight. The following primary antibodies were used: mTOR, p-mTOR, BNIP3L/NIX, and PINK1. Each plate was washed with PBS and incubated at room temperature with a secondary antibody, anti-rabbit IgG conjugated to Alexa Fluor 488 #4412 (Cell

Signaling Technology). For *in vivo* studies, in order to perform immunofluorescence on tissue sections, whole mouse globes were excised, fixed in 1% paraformaldehyde, embedded in O.C.T. Compound Tissue-Plus embedding medium (Thermo Fisher Scientific), and frozen in liquid nitrogen. Tissue blocks were stored at −80 °C. Tissues were sectioned using a cryostat equipped with a cryoJane Tape-Transfer system (Leica). Slides were washed three times in PBS. After washing, tissue sections were fixed with 1% paraformaldehyde and washed again with PBS. Following this, ice cold acetone was used to permeabilize the cells. After rewashing, tissue samples were blocked using 0.5% bovine serum albumin in PBS and then stained with primary and secondary antibodies as described above. Prolong gold anti-fade reagent with DAPI was used to label the nucleus (Invitrogen). A Leica SP8 laser scanning confocal microscope with a 63× oil objective was used to acquire images (Leica Microsystems). Images were sequentially scanned in order to avoid spectral crosstalk between channels.

siRNA knockdown of TSC1

hTCEpi cells were seeded at 50 to 60% confluence into six-well plates and allowed to adhere overnight. Cells were then transfected with double-stranded inhibitory RNA oligonucleotides targeting TSC 1 (FlexiTube GeneSolution, TSC1 #GS7248, Qiagen) using Lipofectamine RNAiMAX (Invitrogen) in antibiotic-free KGM. Twelve pmol of siRNA oligonucleotides targeting TSC1 or nontargeting controls were added to 100 μl KGM and incubated at room temperature for 5 min. The siRNA was combined with 2 μl lipofectamine diluted in 100 μl KGM. This mixture was incubated for 15 min at room temperature. Next, the transfection mixture was added to hTCEpi cells containing 1 ml of KGM. Samples were then incubated for 24 h. At this time point, the transfection media was removed and the cells were cultured in KBM containing 450 mOsm for another 24 h with or without rhIGFBP-3. Allstars negative control siRNA was used as the nontargeting control (Qiagen).

Mitochondrial polarization

To assess mitochondrial polarization, hTCEpi cells were seeded at 70% confluence on 35 mm glass coverslip bottom MatTek dishes (MatTek Corporation) and allowed to adhere overnight. Cells were treated for 6 h in either isotonic KBM or KBM containing 450 mOsm with and without rhIGFBP-3. As an experimental control, hTCEpi cells were treated with 50 μM carbonyl cyanide *m*-chlorophenyl hydrazine in dimethyl sulfoxide for 10 min at 37 °C. Ten minutes prior to the conclusion of the six-hour treatment, cells were treated with either 10 μg/ml of tetraethylbenzimidazolylcarbocyanine iodide (JC-1) dye or 100 nM of MTG (Invitrogen) and 50 nM of TMRE (Abcam). After 10 min, cells were washed three times with PBS. All plates were imaged on a Leica SP8 laser scanning confocal microscope with a 63× oil objective (Leica Microsystems). To maintain the cell culture environment during imaging, an environmental chamber was used (Life Imaging Services). The chamber was kept at 5% CO_2, 37 °C. JC-1–stained monomers were scanned using a 488 nm excitation laser, and JC-1 aggregates (multimers) were scanned using a 561 nm excitation laser. MTG staining was scanned using a 488 nm excitation laser, and TMRE was imaged using a 561 nm excitation laser. Sequential scanning was performed to prevent spectral crosstalk.

Plasmid transfection

For autophagic flux experiments, a GFP-mCherry-*LC3* expression plasmid was transiently expressed in hTCEpi cells according to our published protocol (34). Cells were seeded at 70% confluence on 35 mm glass coverslip bottom MatTek dishes (MatTek Corporation) and allowed to adhere overnight. Transfection was performed with 5 μg of plasmid and 10 μl of P3000 reagent into 125 μl of Opti-MEM medium (Invitrogen). A second mixture was made of 5 μl of Lipofectamine 3000 (Invitrogen) and was also diluted in 125 μl of Opti-MEM medium. These two mixtures were combined after 5 min and allowed to incubate for 15 min before being added to the hTCEpi cells with 1 ml of antibiotic-free KGM. Cells were incubated in the transfection media for 12 h. Cells were then cultured in isotonic KBM or KBM at 450 mOsm with or without rhIGFBP-3 for 6 or 24 h. All cells were imaged with a 63× oil objective on a Leica SP8 laser scanning confocal microscope (Leica Microsystems). Sequential scanning was performed to prevent spectral crosstalk.

Botulinum toxin B–induced aqueous-deficient dry eye mouse model

Animal studies were approved by the Institutional Animal Care and Use Committee at the University of Texas Southwestern Medical Center and complied with the ARVO statement on the use of animals in ophthalmic and vision research. A total of 24 C57BL6 Type N strain mice were used in this study (Charles River). All mice were between the ages of 6 to 8 weeks at the start of the experiments. All groups were age and sex-matched. Mice were randomly assigned to the test or control group. To perform these experiments, we used an aqueous-deficient dry eye model that has been previously described (35, 36). All mice were exposed to the same environmental conditions including stable temperature (21–24 °C) and humidity. Only the right eye was utilized for experiments due to the potential for a sympathetic response between eyes. All mice were screened at baseline prior to the injection for the presence of any ocular surface abnormalities using fluorescein staining and for tear production using a phenol red thread test. Mice were injected with a 33G needle in their right lacrimal gland with either botox (20 mU BTX-B in 0.05 ml 0.9% saline) or a vehicle control (0.05 ml of 0.9% saline, Day 0). Twenty-one days postinjection, the ocular surface of each mouse was treated topically with 10 μl of a solution containing PBS with or without 500 ng/ml of rhIGFBP-3. This was repeated twice daily, every other day for 7 days. After 7 days of treatment, eyes were assessed for corneal staining using fluorescein and tear production using a phenol red thread test. To prevent any

fluorescein uptake from interfering with immunofluorescent imaging, animals were euthanized, and corneal tissue was excised 24 h after the clinical measurements.

Clinical measurements

To analyze ocular surface damage and tear production, corneal fluorescein staining and phenol red thread testing was performed on days 0, 21, and 28. Fluorescein sodium ophthalmic strips (1 mg, BioGel) were used for staining the ocular surface. A slit-lamp biomicroscope with a cobalt blue light and yellow wratten filter was utilized for visualization of the ocular surface. A Sony Cyber Shot camera was fitted to the eye piece of the slit-lamp biomicroscope to obtain pictures for grading. Fluorescein staining was scored using a 0 to 3 scale with 0 indicating no ocular surface staining and 3 indicating severe ocular surface staining according to the NEI grading scale (37). Grading was assessed in all five quadrants and the sum of those quadrants was calculated as the total staining grade. Grading was performed by a blinded observer. A phenol red thread test was then performed to quantify aqueous tear production on days 0, 21, and 28. The tip of the phenol red thread (Zone-Quick) was placed in the lateral canthus of the right eye of the mouse for 15 s while under anesthesia. The length of the thread that turned red after 15 s was measured using a micron ruler.

Statistical analysis

Data is presented as mean ± SD. A Student's t test was used for comparison between two groups. For comparisons among more than two groups, a one-way ANOVA was used. For the comparison of greater than two groups with multiple factors, a two-way ANOVA was performed. For all ANOVAs, appropriate posthoc testing was used. Statistical significance was set at $p < 0.05$.

Data availability

Data for all figures are available in the published article and supplemental material.

Supporting information—This article contains supporting information.

Author contributions—W. S. S., I. J. T., and D. M. R. conceptualization; W. S. S. and I. J. T. data curation; W. S. S. and D. M. R. formal analysis; W. S. S. and D. M. R. funding acquisition; W. S. S., I. J. T., and D. M. R. investigation; W. S. S., I. J. T., and D. M. R. methodology; D. M. R. project administration; D. M. R. resources; D. M. R. supervision; W. S. S., I. J. T., and D. M. R. writing–original draft; W. S. S. and D. M. R. writing–review and editing.

Funding and additional information—This work was supported by NIH/NEI grants EY024546 (D. M. R.), EY029258 (D. M. R.), EY033505 (D. M. R.), F30 EY031559 (W. S. S.), Core grant for Vision Research P30 EY030413, and the Shirley G. and Norman Alweis Endowment Fund for Vision (D. M. R.). The content is solely the responsibility of the authors and does not necessarily represent the official views of the National Institutes of Health.

Conflict of interest—The authors declare that they have no conflicts of interest with the contents of this article.

Abbreviations—The abbreviations used are: DED, dry eye disease; HCjEC, human conjunctival epithelial cell; hTCEpi, human corneal epithelial; IGFBP-3, insulin-like growth factor binding protein-3; KBM, keratinocyte basal media; KGM, keratinocyte growth media; MTG, MitoTracker Green; mTOR, mechanistic target of rapamycin; OCR, oxygen consumption rate; rh, recombinant human; TMRE, tetramethylrhodamine ethyl ester; TSC1, tuberous sclerosis complex 1.

References

1. Craig, J. P., Nichols, K. K., Akpek, E. K., Caffery, B., Dua, H. S., Joo, C. K., *et al.* (2017) TFOS DEWS II definition and classification report. *Ocul. Surf.* **15**, 276–283
2. Research in dry eye: report of the research subcommittee of the International dry eye WorkShop (2007). *Ocul. Surf.* **5**, (2007), 179–193
3. Png, E., Samivelu, G. K., Yeo, S. H., Chew, J., Chaurasia, S. S., and Tong, L. (2011) Hyperosmolarity-mediated mitochondrial dysfunction requires transglutaminase-2 in human corneal epithelial cells. *J. Cell. Physiol.* **226**, 693–699
4. Stookey, J. D., Barclay, D., Arieff, A., and Popkin, B. M. (2007) The altered fluid distribution in obesity may reflect plasma hypertonicity. *Eur. J. Clin. Nutr.* **61**, 190–199
5. Vernia, P., Gnaedinger, A., Hauck, W., and Breuer, R. I. (1988) Organic anions and the diarrhea of inflammatory bowel disease. *Dig. Dis. Sci.* **33**, 1353–1358
6. Schilli, R., Breuer, R. I., Klein, F., Dunn, K., Gnaedinger, A., Bernstein, J., *et al.* (1982) Comparison of the composition of faecal fluid in Crohn's disease and ulcerative colitis. *Gut* **23**, 326–332
7. Pan, Z., Wang, Z., Yang, H., Zhang, F., and Reinach, P. S. (2011) TRPV1 activation is required for hypertonicity-stimulated inflammatory cytokine release in human corneal epithelial cells. *Invest. Ophthalmol. Vis. Sci.* **52**, 485–493
8. Varma Shrivastav, S., Bhardwaj, A., Pathak, K. A., and Shrivastav, A. (2020) Insulin-like growth factor binding protein-3 (IGFBP-3): unraveling the role in mediating IGF-independent effects within the cell. *Front. Cell Dev. Biol.* **8**, 286
9. Titone, R., Zhu, M., and Robertson, D. M. (2019) Mutual regulation between IGF-1R and IGFBP-3 in human corneal epithelial cells. *J. Cell. Physiol.* **234**, 1426–1441
10. Stuard, W. L., Titone, R., and Robertson, D. M. (2022) IGFBP-3 functions as a molecular switch that mediates mitochondrial and metabolic homeostasis. *FASEB J.* **36**, e22062
11. Bogdan, E. D., Stuard, W. L., Titone, R., and Robertson, D. M. (2021) IGFBP-3 mediates metabolic homeostasis during hyperosmolar stress in the corneal epithelium. *Invest. Ophthalmol. Vis. Sci.* **62**, 11
12. Stuard, W. L., Guner, M. K., and Robertson, D. M. (2022) IGFBP-3 regulates mitochondrial hyperfusion and metabolic activity in ocular surface epithelia during hyperosmolar stress. *Int. J. Mol. Sci.* **23**, 4066
13. Martin, L. M., Jeyabalan, N., Tripathi, R., Panigrahi, T., Johnson, P. J., Ghosh, A., *et al.* (2019) Autophagy in corneal health and disease: a concise review. *Ocul. Surf.* **17**, 186–197
14. Onishi, M., Yamano, K., Sato, M., Matsuda, N., and Okamoto, K. (2021) Molecular mechanisms and physiological functions of mitophagy. *EMBO J.* **40**, e104705
15. Barazzuol, L., Giamogante, F., Brini, M., and Calì, T. (2020) PINK1/Parkin mediated mitophagy, Ca(2+) Signalling, and ER-mitochondria contacts in Parkinson's disease. *Int. J. Mol. Sci.* **21**, 1772

16. Marinković, M., and Novak, I. (2021) A brief overview of BNIP3L/NIX receptor-mediated mitophagy. *FEBS Open Bio* **11**, 3230–3236
17. Shivakumar, S., Panigrahi, T., Shetty, R., Subramani, M., Ghosh, A., and Jeyabalan, N. (2018) Chloroquine protects human corneal epithelial cells from desiccation stress induced inflammation without altering the autophagy flux. *Biomed Res. Int.* **2018**, 7627329
18. Ma, S., Yu, Z., Feng, S., Chen, H., Chen, H., and Lu, X. (2019) Corneal autophagy and ocular surface inflammation: a new perspective in dry eye. *Exp. Eye Res.* **184**, 126–134
19. Du, Y., Long, Q., Shi, Y., Liu, X., Li, X., Zeng, J., *et al.* (2015) Insulin-like growth factor binding protein-3 mediates interleukin-24-induced apoptosis through inhibition of the mTOR pathway in prostate cancer. *Oncol. Rep.* **34**, 2273–2281
20. Li, Y., Liu, H., Zeng, W., and Wei, J. (2017) Edaravone protects against hyperosmolarity-induced oxidative stress and apoptosis in primary human corneal epithelial cells. *PLoS One* **12**, e0174437
21. Luo, L., Li, D. Q., and Pflugfelder, S. C. (2007) Hyperosmolarity-induced apoptosis in human corneal epithelial cells is mediated by cytochrome c and MAPK pathways. *Cornea* **26**, 452–460
22. Sekine, S., and Youle, R. J. (2018) PINK1 import regulation; a fine system to convey mitochondrial stress to the cytosol. *BMC Biol.* **16**, 2
23. Ladage, P. M., Yamamoto, K., Ren, D. H., Li, L., Jester, J. V., Petroll, W. M., *et al.* (2001) Proliferation rate of rabbit corneal epithelium during overnight rigid contact lens wear. *Invest. Ophthalmol. Vis. Sci.* **42**, 2804–2812
24. Palikaras, K., Lionaki, E., and Tavernarakis, N. (2018) Mechanisms of mitophagy in cellular homeostasis, physiology and pathology. *Nat. Cell Biol.* **20**, 1013–1022
25. Fabiani, C., Barabino, S., Rashid, S., and Dana, M. R. (2009) Corneal epithelial proliferation and thickness in a mouse model of dry eye. *Exp. Eye Res.* **89**, 166–171
26. Liu, G. Y., and Sabatini, D. M. (2020) mTOR at the nexus of nutrition, growth, ageing and disease. *Nat. Rev. Mol. Cell Biol.* **21**, 183–203
27. Wang, Y., and Zhang, H. (2019) Regulation of autophagy by mTOR signaling pathway. *Adv. Exp. Med. Biol.* **1206**, 67–83
28. Robertson, D. M., Li, L., Fisher, S., Pearce, V. P., Shay, J. W., Wright, W. E., *et al.* (2005) Characterization of growth and differentiation in a telomerase-immortalized human corneal epithelial cell line. *Invest. Ophthalmol. Vis. Sci.* **46**, 470–478
29. Hori, Y., Spurr-Michaud, S., Russo, C. L., Argüeso, P., and Gipson, I. K. (2004) Differential regulation of membrane-associated mucins in the human ocular surface epithelium. *Invest. Ophthalmol. Vis. Sci.* **45**, 114–122
30. Delgado, O., Kaisani, A. A., Spinola, M., Xie, X. J., Batten, K. G., Minna, J. D., *et al.* (2011) Multipotent capacity of immortalized human bronchial epithelial cells. *PLoS one* **6**, e22023
31. Vaughan, M. B., Ramirez, R. D., Wright, W. E., Minna, J. D., and Shay, J. W. (2006) A three-dimensional model of differentiation of immortalized human bronchial epithelial cells. *Differentiation* **74**, 141–148
32. Gipson, I. K., Spurr-Michaud, S., Argüeso, P., Tisdale, A., Ng, T. F., and Russo, C. L. (2003) Mucin gene expression in immortalized human corneal-limbal and conjunctival epithelial cell lines. *Invest. Ophthalmol. Vis. Sci.* **44**, 2496–2506
33. Wu, Y. C., Zhu, M., and Robertson, D. M. (2012) Novel nuclear localization and potential function of insulin-like growth factor-1 receptor/insulin receptor hybrid in corneal epithelial cells. *PLoS One* **7**, e42483
34. Titone, R., and Robertson, D. M. (2020) Insulin receptor preserves mitochondrial function by binding VDAC1 in insulin insensitive mucosal epithelial cells. *FASEB J.* **34**, 754–775
35. Calonge, M., Enríquez-de-Salamanca, A., Diebold, Y., González-García, M. J., Reinoso, R., Herreras, J. M., *et al.* (2010) Dry eye disease as an inflammatory disorder. *Ocul. Immunol. Inflamm.* **18**, 244–253
36. Lin, B. W., Chen, M. Z., Fan, S. X., Chuck, R. S., and Zhou, S. Y. (2014) Effect of 0.025% FK-506 eyedrops on botulinum toxin B-induced mouse dry eye. *Invest. Ophthalmol. Vis. Sci.* **56**, 45–53
37. Lemp, A. (1995) Report of the National Eye Institute/Industry workshop on clinical trials in dry eyes. *CLAO J.* **21**, 221–232